

# Temporal dynamics of basal ganglia response and connectivity during verbal working memory

Catherine Chang,<sup>a,b,\*</sup> Sonia Crottaz-Herbette,<sup>b</sup> and Vinod Menon<sup>b,c,d,\*</sup>

<sup>a</sup>Department of Electrical Engineering, Stanford University, Stanford, CA 94305, USA

<sup>b</sup>Department of Psychiatry and Behavioral Sciences, Stanford University School of Medicine, Stanford, CA 94305, USA

<sup>c</sup>Program in Neuroscience, Stanford University School of Medicine, Stanford, CA 94305, USA

<sup>d</sup>Neuroscience Institute at Stanford, Stanford University School of Medicine, Stanford, CA 94305, USA

Received 24 April 2005; revised 17 August 2006; accepted 21 August 2006  
Available online 18 December 2006

Research on the neural basis of working memory (WM) has generally focused on neocortical regions; comparatively little is known about the role of subcortical structures. There is growing evidence that the basal ganglia are involved in WM, but their contribution to different component processes of WM is poorly understood. We examined the temporal dynamics of basal ganglia response and connectivity during the encoding, maintenance and response phases of a Sternberg WM task. During the encoding and maintenance phases, WM-load-dependent activation was observed in the left anterior caudate, anterior putamen and globus pallidus; activation in the right anterior caudate was observed only during the maintenance phase. During the response phase, the basal ganglia were equally active in both the high-load and low-load WM conditions. Caudate and putamen activations were primarily localized to the (rostral) associative parts of the basal ganglia, consistent with the putative role of these regions in cognitive processing. Effective connectivity analyses revealed increased WM-load-dependent interaction of the left anterior caudate with the left posterior parietal cortex during all three phases of the task; with the visual association cortex, including the fusiform gyrus and inferior temporal gyrus, only during the encoding phase; with the ventrolateral prefrontal cortex during the encoding and maintenance phases; with the pre-supplementary motor area during the maintenance and response phases; and with the dorsolateral prefrontal and anterior cingulate cortices only during the response phase. Taken together with known neuroanatomy of the basal ganglia, these results suggest that the anterior caudate helps to link signals in distinct functional networks during different phases of the WM task. Our study offers new insight into the integrative and adaptive role of the basal ganglia in higher cognitive function.

© 2006 Elsevier Inc. All rights reserved.

*Keywords:* Basal ganglia; Caudate; Brain connectivity; Sternberg; fMRI

---

\* Corresponding authors. Department of Psychiatry and Behavioral Sciences, 780 Welch Rd, Room 201, Stanford University School of Medicine, Stanford, CA 94305, USA.

*E-mail addresses:* [catie@stanford.edu](mailto:catie@stanford.edu) (C. Chang), [menon@stanford.edu](mailto:menon@stanford.edu) (V. Menon).

Available online on ScienceDirect ([www.sciencedirect.com](http://www.sciencedirect.com)).

1053-8119/\$ - see front matter © 2006 Elsevier Inc. All rights reserved.  
doi:10.1016/j.neuroimage.2006.08.056

## Introduction

It is now well established that the basal ganglia (BG) play an important role in motor control and sequencing (Alexander et al., 1986; Aldridge and Berridge, 1998). Beyond this, there is growing evidence that the BG are specifically involved in cognitive operations (Alexander et al., 1986; Graybiel, 1997; Ravizza and Ivry, 2001), such as working memory (WM), independent of motor and sensory operations (Owen et al., 1997; Postle and D'Esposito, 1999a,b; Skeeel et al., 2001; Lewis et al., 2004). WM, the ability to maintain and manipulate information during a short interval (Baddeley, 1997; Goldman-Rakic, 1999), is fundamental to many cognitive functions, and its neural basis has been the subject of numerous investigations (Baddeley, 2003). Most of these studies have focused on the role of cortical regions, notably the dorsolateral and ventrolateral prefrontal and posterior parietal cortices (Owen et al., 1996; Fletcher and Henson, 2001). Much less is known about the role of the BG, with which these cortical regions are tightly linked (Alexander et al., 1986; Middleton and Strick, 2002). The aim of our study is to investigate more thoroughly the role of the BG in verbal WM using an event-related functional magnetic resonance imaging (fMRI) task along with network analysis of BG responses during different stages of WM.

BG involvement in WM has been demonstrated in animal studies which found severe performance impairments following striatal lesions (Rosvold and Delgado, 1956; Dean and Davis, 1959; Battig et al., 1960; Divac et al., 1967; Goldman and Rosvold, 1972). Electrophysiological studies have also reported enhanced neuronal firing in the BG during visuo-spatial WM tasks (Stamm, 1969; Mordinov, 1981; Alexander et al., 1986; Hikosaka et al., 1989; Apicella et al., 1992). Animal studies have almost exclusively focused on visuo-spatial WM, and hence less information is available concerning non-spatial forms of WM. In patients with Parkinson's disease, reduced dopamine in the striatum has been associated with selective impairments of visuo-spatial WM (Morris et al., 1988; Bradley et al., 1989; Cooper et al., 1991; Owen et al., 1998; Dagher et al., 2001; Lewis et al., 2003) as well

as non-spatial or verbal WM (Owen et al., 1997). These studies suggest that the BG are involved in both spatial and non-spatial WM processing. However, they do not provide information about the precise anatomical locus of BG deficits that impact specific stages of WM operations, especially for the less well-studied non-spatial forms of WM.

Consistent with animal lesion and human patient studies, several human neuroimaging studies have found increased activation in the BG during verbal WM. Activation of the caudate has been reported in complex WM tasks, such as those in which subjects are required to match a probe with a test item presented two steps back (D'Esposito et al., 1998; Crottaz-Herbette et al., 2004). However, the complexity of this task and the requirements of maintaining as well as manipulating information in memory have precluded determination of the precise role of the caudate in WM. The Sternberg task (Sternberg, 1966) and its variants have been used to more closely examine the role of different brain regions in the different stages of WM. The Sternberg task consists of an “encoding” phase, during which stimuli are presented and must be committed to memory; a “maintenance” phase, during which the information is held in short-term memory; and a “response” or “probe” phase, during which the subject retrieves the stored information, compares it with a probe and makes a response. Here again, the focus of previous studies has primarily been on cortical structures (Elliott and Dolan, 1999; Postle and D'Esposito, 1999a,b; Rypma et al., 1999; Chein and Fiez, 2001; Manoach et al., 2003; Cairo et al., 2004).

Using a modified Sternberg task involving letters, Lewis et al. (2004) showed that activation in the caudate was greater when subjects had to manipulate, as opposed to simply maintain, information in WM. This study did not specifically examine activation during the encoding, maintenance and retrieval phases. The use of a small sample size, and an older group of individuals (50–70 years old) with an unspecified mean age, also raises concerns regarding the generalizability of the findings because it is not clear to what extent the findings were confounded by aging effects. Two recent studies have used larger sample sizes to investigate brain responses during all three phases of the Sternberg task (Manoach et al., 2003; Cairo et al., 2004). Although the focus of both these studies was predominantly cortical, they also reported differential responses in the BG. Manoach et al. (2003) found activation in the globus pallidus during the response phase only, whereas Cairo et al. (2004) observed activation in the caudate, putamen and globus pallidus during the encoding phase, and in the putamen during the maintenance phase.

We used event-related fMRI, and a Sternberg task with visual verbal stimuli, to investigate the temporal dynamics of BG responses during the encoding, maintenance and response phases of WM. We compared BG activation and effective connectivity during a high-load WM condition with those during a low-load WM condition. This allowed us to examine, for the first time, network functions of the BG during WM after controlling for factors including task context, low-level memory, and sensory and motor processing. One aim of our study was to resolve contradictory findings observed in previous studies. More importantly, we sought to extend findings from previous studies in novel and important ways by investigating the interactions of BG with the lateral prefrontal and parietal cortices, the pre-supplementary motor area (pre-SMA) and the anterior cingulate cortex (ACC)—brain areas well known to be involved in manipulating and maintaining information in WM, as well as in top-down attention control and

response preparation (Funahashi et al., 1989; Petrides et al., 1993; Owen et al., 1996; Braver et al., 1997; Humberstone et al., 1997; Rowe et al., 2000; Crottaz-Herbette and Menon, 2006) during different stages of the WM task.

We modified the standard Sternberg task in a manner that is particularly relevant to the study of BG function. One problem with the standard task design (Manoach et al., 2003; Cairo et al., 2004), particularly for interpreting findings of brain imaging studies, is that even for explicitly non-spatial tasks, the stimuli to be encoded into memory are presented simultaneously at multiple spatial locations. This requires the subject to make multiple eye movements to encode the stimulus set. The BG, in addition to their well-known role in movement, also control purposive saccadic eye movements (Hikosaka et al., 2000). Thus, a task requiring saccades would confound a network analysis since basal ganglia pathophysiology can influence eye movement processing in the frontal cortex (Armstrong et al., 2002). Our study eliminated these problems by presenting the stimuli to be encoded one at a time, in quick succession.

It is well known that the general linear model (GLM) analysis of distinct phases of the Sternberg task is susceptible to multicollinearity, as the events of interest are closely spaced and cannot be temporally randomized to improve statistical efficiency. We did not vary the length of the maintenance phase, as delays of different lengths have been shown to elicit qualitatively different patterns of brain activation (Elliott and Dolan, 1999). Introducing small changes in delay-length may not result in significant increases in statistical power, particularly at the group level. If delays are varied over longer durations, however, brain processes engaged by the task are likely to differ from trial to trial and there would be no way of disentangling WM load effects resulting from stimulus set size (as conceptualized in this study) from those resulting from variable delays. Hence, the statistical power gained from varying the duration of delay phase in the Sternberg task must be weighed against changes in brain responses elicited by such variable delays. To minimize collinearity, events corresponding to each phase were modeled as impulses spaced 4 s apart. Furthermore, to explore the detection power and rate of false positives, we conducted simulations using AR(1) noise and signal-to-noise ratio of 0.2 and higher. Our simulations sought to assess the accuracy with which our GLM covariates could detect activation specific to a particular phase of the Sternberg task, as well as the rate of misattribution of activation to temporally adjacent phases. The results demonstrate an ability to discern activation specific to each phase.

We examined BG responses and effective connectivity (Friston et al., 1997) to test the hypotheses that (1) WM-load-dependent activation would be observed in the BG, especially the anterior caudate during all three phases of the Sternberg WM task, (2) BG responses would be more tightly coupled to the PFC and the PPC, pre-SMA and ACC during the high-load, compared to the low-load, WM condition, and (3) BG connectivity would reflect integration of different cortical circuits during each of the three phases.

## Materials and methods

### Subjects

Fourteen healthy right-handed adults (7 females, 7 males, ages: 18–32 years) participated in this study after giving written

informed consent. Handedness was assessed using the Edinburgh test (Oldfield, 1971). All protocols used in this study were approved by the human subjects committee at Stanford University School of Medicine.

### Task

Subjects performed a variant of the Sternberg task (Sternberg, 1966). Each trial consisted of one of two conditions: a high-load or a low-load WM condition (Fig. 1). In each trial, subjects were first presented with a 500 ms fixation cross in the middle of the screen followed by an encoding phase in which five target stimuli were presented consecutively for 425 ms each, with a 75 ms interval between consecutive stimuli. This was followed by a 5 s maintenance (delay) phase during which a fixation cross at the center of a blank screen was displayed. Immediately following the maintenance phase, a probe stimulus lasting 500 ms was presented. Subjects were instructed to press a button with the right index finger if the probe stimulus was part of the target set (a match), and with the right middle finger if it was not. 50% of the trials were matches. The inter-trial interval (onset to onset) was 20 s in order to allow the hemodynamic response to return close to baseline between trials. Stimuli were numbers (0–9) displayed in the center of the screen. In the high-load WM condition, the target stimulus set consisted of five different numbers (e.g. “4 2 7 3 9”), while in the low-load WM condition, the same number (e.g. “2 2 2 2 2”) comprised all five targets. Two sessions were used, with 24 trials within each session. High- and low-load WM trials were randomly intermixed within sessions. Each session began with a 30 s rest interval to allow the fMRI signals to equilibrate. The task was programmed using Psyscope (Cohen et al., 1993) on a Macintosh (Sunnyvale, CA) computer.

### Behavioral data analysis

Accuracy and reaction time (RT) were recorded for each trial. Accuracy refers to the percentage of trials (match and non-match trials) in which the subject responded correctly with an appropriate button push. Performances in the high- and low-load WM conditions were compared using *t*-tests for the accuracy and RT.

### fMRI acquisition

Images were acquired on a 1.5 T GE Signa scanner with Echospeed gradients using a standard whole head coil. A custom-

built head holder was used to prevent head movement. 28 axial slices (4 mm thick, 0.5 mm skip) parallel to the anterior and posterior commissure covering the whole brain were imaged with a temporal resolution of 2 s using a T2\* weighted gradient echo spiral pulse sequence (TR=2000 ms, TE=40 ms, flip angle=89° and 1 interleave) (Glover and Lai, 1998). The field of view was 200 mm, and the acquisition voxel size was 3.75×3.75×4.5 mm. To aid in localization of functional data, a high-resolution T1-weighted spoiled grass gradient recalled (SPGR) 3D MRI sequence with the following parameters was used: TR=35 ms; TE=6 ms; flip angle=45°; 24 cm field of view; 124 slices in coronal plane; 256×192 matrix. Initiation of scan and task was synchronized using a TTL pulse delivered to the scanner timing microprocessor board from a “CMU Button Box” microprocessor (<http://psyscope.psy.cmu.edu>) connected to the Macintosh. Visual stimuli were presented at the center of a screen using a custom-built magnet compatible projection system (Resonance Technology, CA).

### Image preprocessing

Images were reconstructed, by inverse Fourier transforms, into 64×64×28 image matrices. fMRI data were pre-processed using SPM2 (<http://www.fil.ion.ucl.ac.uk/spm>). Slice timing correction was applied followed by motion correction using least squares minimization and without higher-order corrections for spin history. Images were then resampled every 2 mm using sinc interpolation, normalized to stereotaxic Talairach coordinates (Talairach and Tournoux, 1988) and smoothed with a 4 mm Gaussian kernel to decrease spatial noise (post-processing voxel size: 2×2×2 mm).

### fMRI statistical analysis

Statistical analysis at the individual subject level was performed using the GLM, as implemented in SPM2. Separate regressors were constructed for each phase of the Sternberg task (encoding, maintenance, response) for each of the two conditions (low load and high load). BOLD responses during the encoding, maintenance and response phases were modeled as impulses of neural activity convolved with the canonical HRF. Impulses were placed at the onset of the encoding phase, 1.5 s after the onset of the delay phase and 0.5 s after the onset of the response phase. This approach separates the onsets of temporally adjacent covariates by 4 s in order to minimize collinearity (Zarahn et al., 1997) and has been used successfully in previous studies (Gazzaley et al., 2004). An intercept term was included in the GLM to model the effect of block. Low frequency noise was removed with a high pass filter (cutoff period 120 s) applied to the fMRI time series at each voxel, and an AR(1) model was fit to the residuals to account for intrinsic temporal autocorrelations. No global scaling was performed.

To examine response differences between the high- and low-load conditions across the trials as a whole – that is, without separately modeling the encoding, maintenance and response phases – we also performed a separate analysis using two regressors (one modeling high-load trials, and one modeling low-load trials) along with an intercept term. Here, the BOLD response for each trial was modeled as a 10 s boxcar function convolved with the canonical HRF.

Group analysis was performed using a random-effects model with a two-stage hierarchical procedure. This model estimates the error variance for each condition of interest across subjects, rather than across scans, and therefore provides a stronger generalization

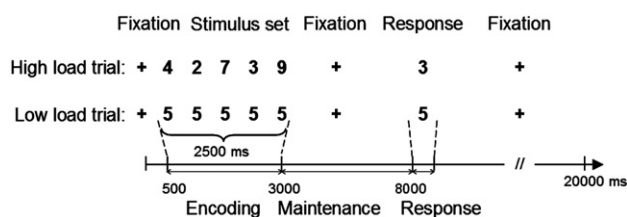


Fig. 1. Schematic diagram of the task showing stimuli and the timing of high- and low-load WM trials. Each trial lasted 20 s and began with the presentation of a fixation point for 500 ms followed by 5 successive numbers for 2.5 s (425 ms per number, with a 75 ms interval between consecutive stimuli) and a maintenance interval of 5 s. A probe was presented for 500 ms at the end of the maintenance period. In the final 11.5 s of the trial, subjects passively viewed a fixation point at the center of the screen.

to the population from which data are acquired (Friston et al., 1995). In the first stage, *t*-contrast images for each subject were first generated for all effects of interest: (i)  $encoding_{high-load} - encoding_{low-load}$ , (ii)  $maintenance_{high-load} - maintenance_{low-load}$  and (iii)  $probe_{high-load} - probe_{low-load}$  when the three phases were modeled separately, and ( $high-load - low-load$ ) when the three phases were not modeled separately. In the second stage, the individual contrast images were analyzed with the GLM, and a one-sample *t*-test was used to determine group activation for each effect. The *t*-statistics were normalized to *Z* scores, and significant clusters of activation were determined using the joint expected probability distribution of height ( $Z > 2.65$ ,  $df = 13$ ;  $p < 0.01$ ) and extent ( $p < 0.01$ ) thresholds of *Z* scores (Poline et al., 1997), corrected for multiple comparisons.

Activation foci were superimposed on high-resolution T1-weighted images, and the locations of the activation were interpreted using known neuroanatomical landmarks (Mai et al., 1997; Duvernoy et al., 1999). MNI coordinates were transformed to Talairach coordinates using a non-linear transformation (Brett, 2000).

### Simulations

We performed simulations to confirm that the covariates used in our GLM could successfully detect activation corresponding to individual task phases. We examined the ideal situation in which there is no mismatch between the actual and modeled HRFs. We simulated the hemodynamic response of a single voxel activated under two different conditions: (i) the high-load encoding phase alone, and (ii) both the high-load encoding and high-load maintenance phases. In condition (i) we examined whether activation would be detected during the maintenance phase when in fact there was no true activation. In condition (ii) we examined whether activation could be detected in both encoding and maintenance phases.

The voxel-wise response was modeled by impulses convolved with the canonical HRF, where impulses for the encoding and maintenance phases were separated by 4 s. To this response we added temporally autocorrelated noise (AR(1) parameter 0.2) with signal-to-noise ratios ranging from 0.1 to 0.6. The resulting signal was regressed against our model (see the section fMRI statistical analysis), and a *t*-test was used to determine the significance of activation during the encoding and maintenance phases. Five hundred independent iterations were performed. Simulations were implemented in MATLAB (The Mathworks Inc., Natick, MA).

### Regions of interest

Regions of interest (ROIs) analyses were conducted for the BG nuclei. First, ROIs encompassing the caudate, putamen and globus pallidus (GP) were hand-drawn separately in each hemisphere on the group averaged T1-weighted structural MRI image. ROIs were drawn using MRICRO ([www.mricro.com](http://www.mricro.com)). The ROIs were then drawn separately on the axial plane of the average brain image in accordance with standard brain atlases (Duvernoy et al., 1999; Talairach and Tournoux, 1988). Drawn ROIs were also examined and corrected on the coronal and sagittal plane in order to determine reliability of axial drawings.

Left and right caudate regions began at Talairach *z*-coordinate of  $-10$  and ended at  $+22$ . The anterior commissure (AC) and the termination of the optic tract posterior to the caudate defined the

ventral extent of the ROI. The dorsal extent of the caudate was marked by the closure of the anterior and posterior lateral ventricles, and when the caudate could no longer be seen clearly (Magnotta et al., 1999). The left and right putamen ROIs began at Talairach *z*-coordinate of  $-10$  and ended at  $+12$ . Tracing of the putamen was defined by the ventral extent of the head of the caudate while the joining of the anterior and posterior internal capsule defined the dorsal extent of the ROI. The medial boundary of the putamen was defined by the border of the GP; tracing terminated when the putamen could no longer be defined accurately (Magnotta et al., 1999). The left and right GP ROI began at Talairach *z*-coordinate  $-4$  and ended at  $+6$ . The ventral extent of the GP ROI was defined by the joining of the AC across the left and right hemispheres. The dorsal extent of the GP was defined by the posterior internal capsule between the putamen and thalamus, and the disappearance of gray matter between the putamen and posterior internal capsule.

### Effective connectivity

Effective connectivity analysis (Friston et al., 1997) was used to examine the WM-load-dependent interaction of the BG with other brain regions during the various stages of WM processing. Effective connectivity is defined here as the influence of one region upon another, after discounting the influence of task-related effects as well as the effects of a common driving input.

A cluster in the left anterior caudate (center of mass:  $x = -16$ ,  $y = 14$ ,  $z = 8$ ) was selected as the seed region for the effective connectivity analysis as it exhibited strong activation at the group level during the maintenance phase. The anterior caudate is unambiguously part of the associative, rather than the motor aspects of the BG (Postuma and Dagher, 2006); furthermore, in our task, movement was matched between the high-load and low-load WM tasks. This ROI was defined by taking the intersection of the thresholded ( $p < 0.01$ , corrected for multiple comparisons) functional activation during the maintenance phase with the anatomical left anterior caudate ROI. For each subject, the average time series were extracted from the seed region, and subsequently mean-corrected, high-pass-filtered ( $f < 1/120$ ) and smoothed with the canonical HRF kernel. No deconvolution or other transforms were performed on the time series. We then constructed bilinear regressors corresponding to the phase-dependent physiological interaction (PI) of the seed region. For each of the three phases, we constructed one PI regressor by taking the pointwise (Hadamard) product between (a) the time series of the seed region and (b) the difference between the high- and low-load task regressors for that phase.

The GLM used in the effective connectivity analysis for each subject included 11 regressors: the 3 PI regressors described in the above paragraph, 1 regressor corresponding to the filtered time series from the seed region, the 6 task- and phase-related regressors described in the section fMRI statistical analysis, and 1 intercept term. Our analysis of effective connectivity was thus specific for BG-modulated influences that occurred over and above any task.

For each of the three phases, brain regions that showed significant PPI effects were determined by testing for positive slopes of the phase-specific PI regressor (i.e. by applying a *t*-contrast that was 1 for the PPI regressor of the respective phase and 0 for all other effects). Subject-specific contrast images were determined and then entered into random effects group analyses. This second level connectivity analysis allowed us to extend inferences to the

population from which the data were acquired. An inclusive mask was used to limit the analysis to voxels that showed task-related activations (with a  $p < 0.05$  uncorrected height and extent thresh-

old) in the phase of interest. The significance of the results was assessed at a  $p < 0.05$  uncorrected threshold, due to the reduced size of the search volumes.

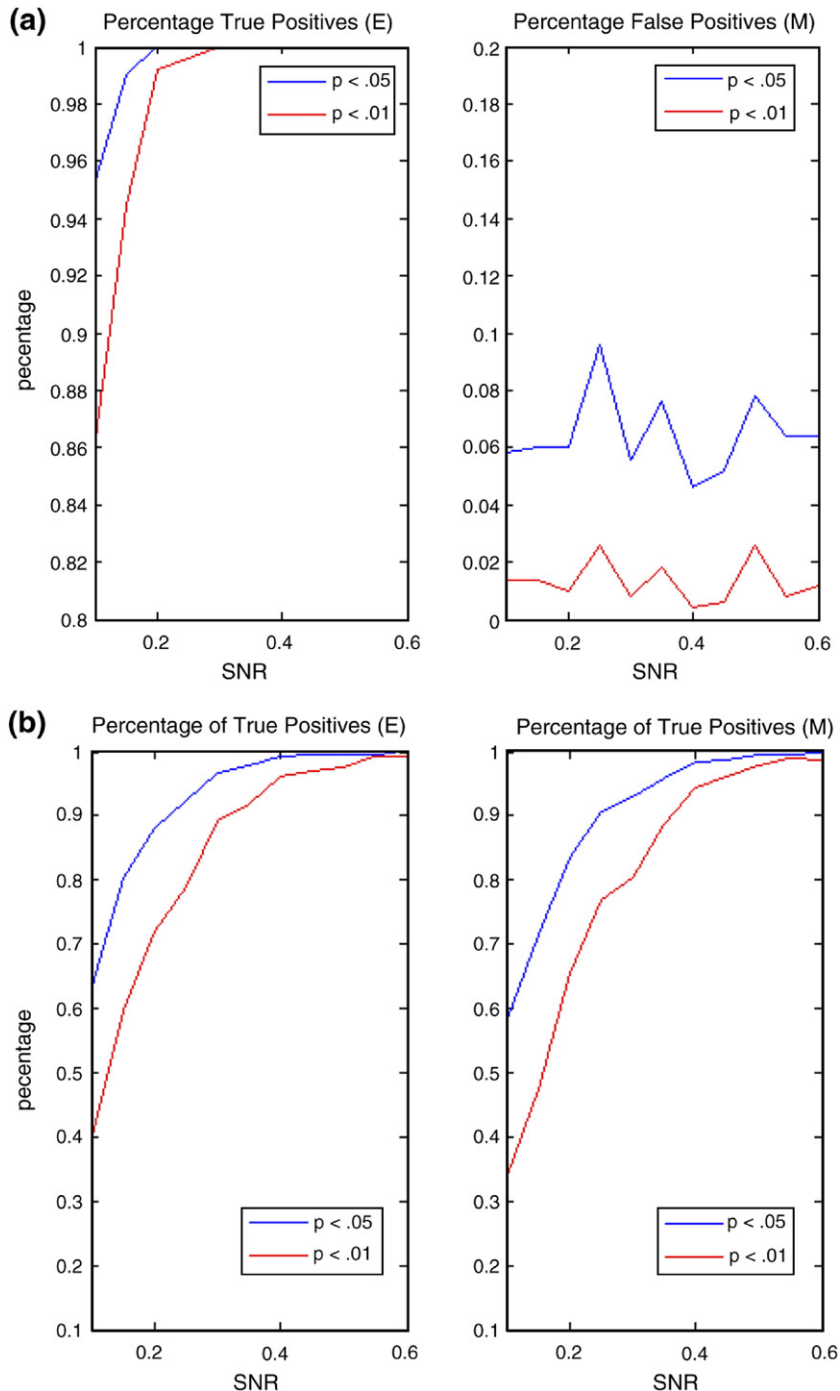


Fig. 2. True and false positive detection rates of simulated encoding and maintenance responses as a function of signal to noise ratio (SNR). Single-voxel responses were simulated under various experimental conditions that mimicked expected patterns of brain responses. (a) (Left) True positive detection rate of encoding-related responses as a function of SNR, when the simulated voxel was active only during the encoding phase. Note that the rate of correctly detected encoding-related activation remains above 95% for  $p < 0.05$  (above 86% for  $p < 0.01$ ). (Right) False positive detection rate of maintenance-related responses as a function of SNR, when the simulated voxel was active only during the encoding phase. Note that the false positive rate remains below 10% for  $p < 0.05$  (under 3% for  $p < 0.01$ ) and is relatively constant for the specified SNR range. (b) (Left) True positive detection rate of encoding-related responses as a function of SNR, when the simulated voxel was active during both the encoding and maintenance phases. (Right) True positive detection rate of maintenance-related responses as a function of SNR, when the simulated voxel was active during both the encoding and maintenance phases.

## Results

### Behavioral performance

Performance levels were high in both WM conditions. Accuracy (mean±standard error) was 97.62%±0.84% in the low-load WM condition and 96.43%±1.44% in the high-load WM condition. RTs, computed relative to the presentation of the probe stimulus, were 1030 ms±65.59 ms in the low-load WM condition and 1243 ms±52.67 ms in the high-load WM condition. Performances for the high- and low-load WM conditions were compared using paired *t*-tests. RTs were significantly shorter for the low-load WM condition compared to the high-load WM condition ( $t(13)=4.72$ ;  $p=0.0004$ ). Accuracy was not significantly different between the two conditions ( $t(13)=0.84$ ;  $p=0.41$ ).

### Simulations

In condition (i), wherein the simulated voxel was active during the encoding phase only, the rate of correctly detected encoding-related activation remained above 95% for  $p<0.05$  (above 86% for  $p<0.01$ ) and rose sharply (Fig. 2a); the rate of misattribution to the maintenance phase remained below 10% for  $p<0.05$  (under 3% for  $p<0.01$ ) and was relatively constant for the specified SNR range (Fig. 2b). In condition (ii), wherein the simulated voxel was active during both the encoding and maintenance phases, successful

detection of both encoding- and maintenance-related activation increased sharply as a function of SNR (Figs. 2c and d). Our simulations treated the ideal scenario, in which no discrepancies exist between the actual and modeled HRFs; however, we acknowledge that mismatch between actual and modeled HRF with respect to parameters such as latency, time-to-peak and dispersion could affect the ability of the GLM to disambiguate responses to the component phases. On the other hand, such mismatches are likely to vary across subjects (Handwerker et al., 2004) thereby increasing error variance and reducing detection power at the group level. This is likely to increase Type II rather than Type I error. While some previous studies using the Sternberg paradigm have introduced 1–2 s jitter in the length of the maintenance phase (Manoach et al., 2003; Cairo et al., 2004; Kirschen et al., 2005), the amount of increased detection power is unclear. Jittering the length of the maintenance phase beyond a couple of seconds, on the other hand, fundamentally changes the nature of the memory task. Such design and analysis issues are important and currently unresolved in the field, warranting further investigation.

### Overall WM-load-related activation

We first compared activation in the high-load versus low-load WM conditions within the entire duration of each trial (i.e. without separating responses to the encoding, maintenance and retrieval phases of the task). As predicted, we found significant activation of

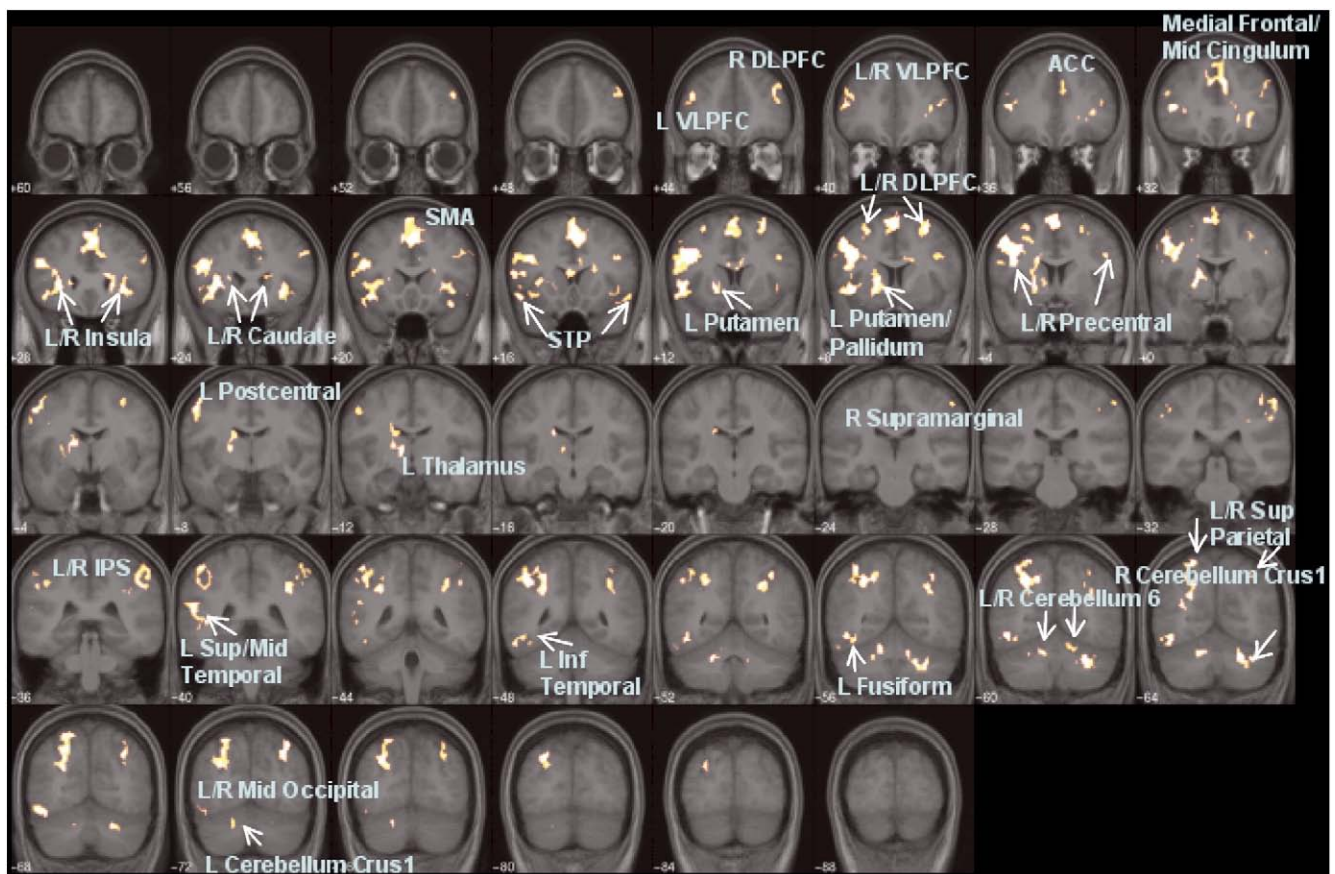


Fig. 3. Brain areas that showed significant WM-load-dependent activation (high-load>low-load) averaged across all three phases of the task. Each cluster was significant after correction for multiple spatial comparisons ( $p<0.01$ ). Activations are shown superposed on group-averaged, spatially normalized, T1-weighted structural images.

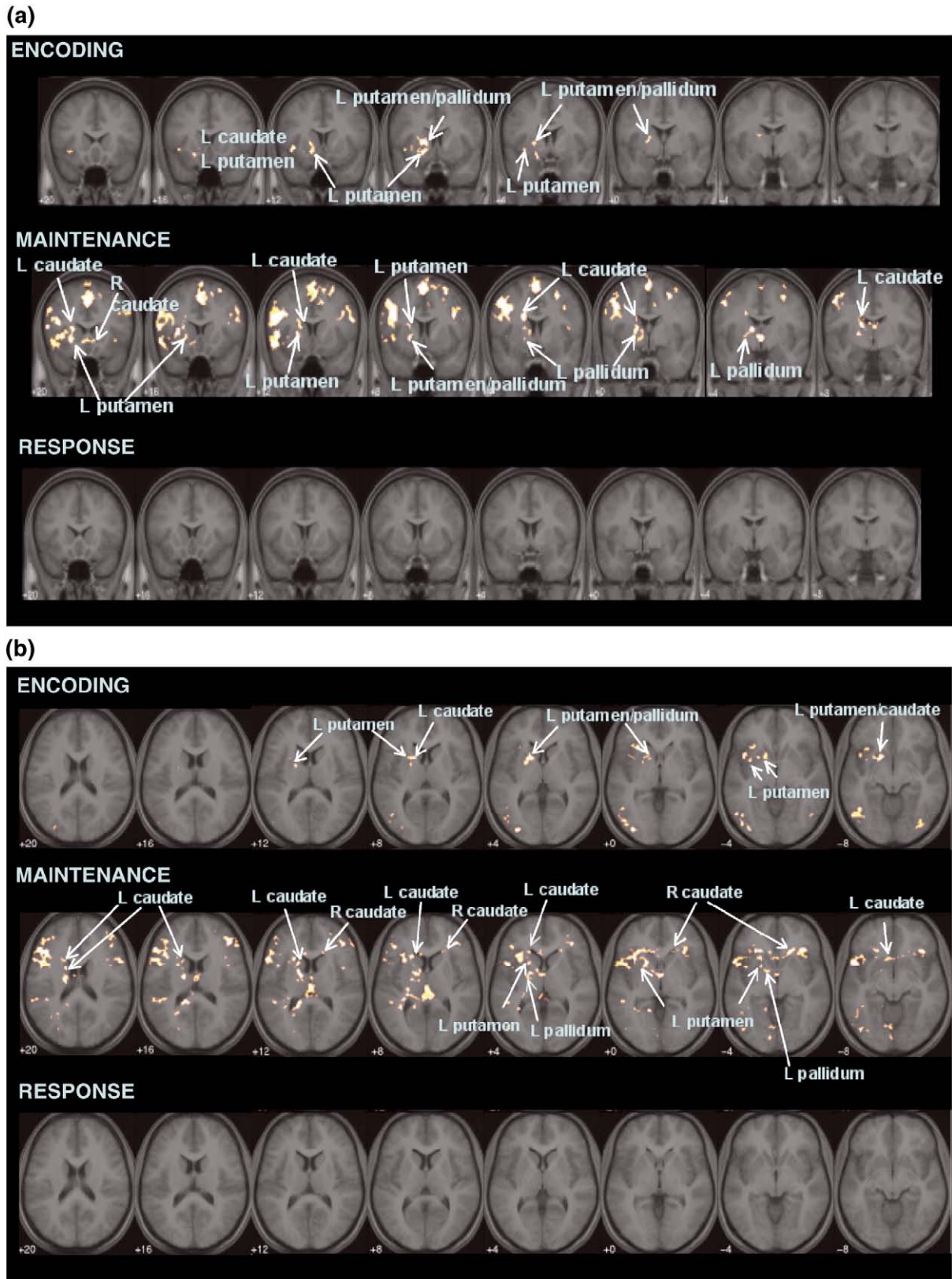


Fig. 4. Specific basal ganglia nuclei that showed significant WM-load-dependent activation (high-load>low-load) during the encoding (top), maintenance (middle) and response (bottom) phases of the WM task. Each cluster was significant after correction for multiple spatial comparisons ( $p < 0.01$ ). Activations are shown superposed on group-averaged, spatially normalized, T1-weighted structural images. Both coronal (a) and axial (b) slices are shown. Significant WM-load-dependent basal ganglia activation was observed during the encoding and maintenance phases, but not during the response phase.

the BG, including the caudate, putamen and globus pallidus. These responses were predominantly localized to the left hemisphere. We also found significant activation in the VLPFC, DLPFC, pre-SMA, fusiform gyrus/inferior temporal gyrus (FG/ITG), ACC and PPC (Fig. 3).

*WM-load-related activation in each phase*

We then compared high- and low-load WM conditions in each of the three phases of the task. This analysis revealed significant

load-dependent BG activation during the encoding and maintenance phases. Activation of the left caudate, putamen and globus pallidus was observed during both the encoding and maintenance phases, and activation in the right caudate was observed during the maintenance phase (Fig. 4). Activations within the caudate and putamen were mainly anterior to the anterior commissure.

Event time courses for the left anterior caudate, anterior putamen and pallidum and the right anterior caudate ROIs are shown in Fig. 5. It is evident that all four of these ROIs exhibit stronger responses in the high-load, compared to the low-load,

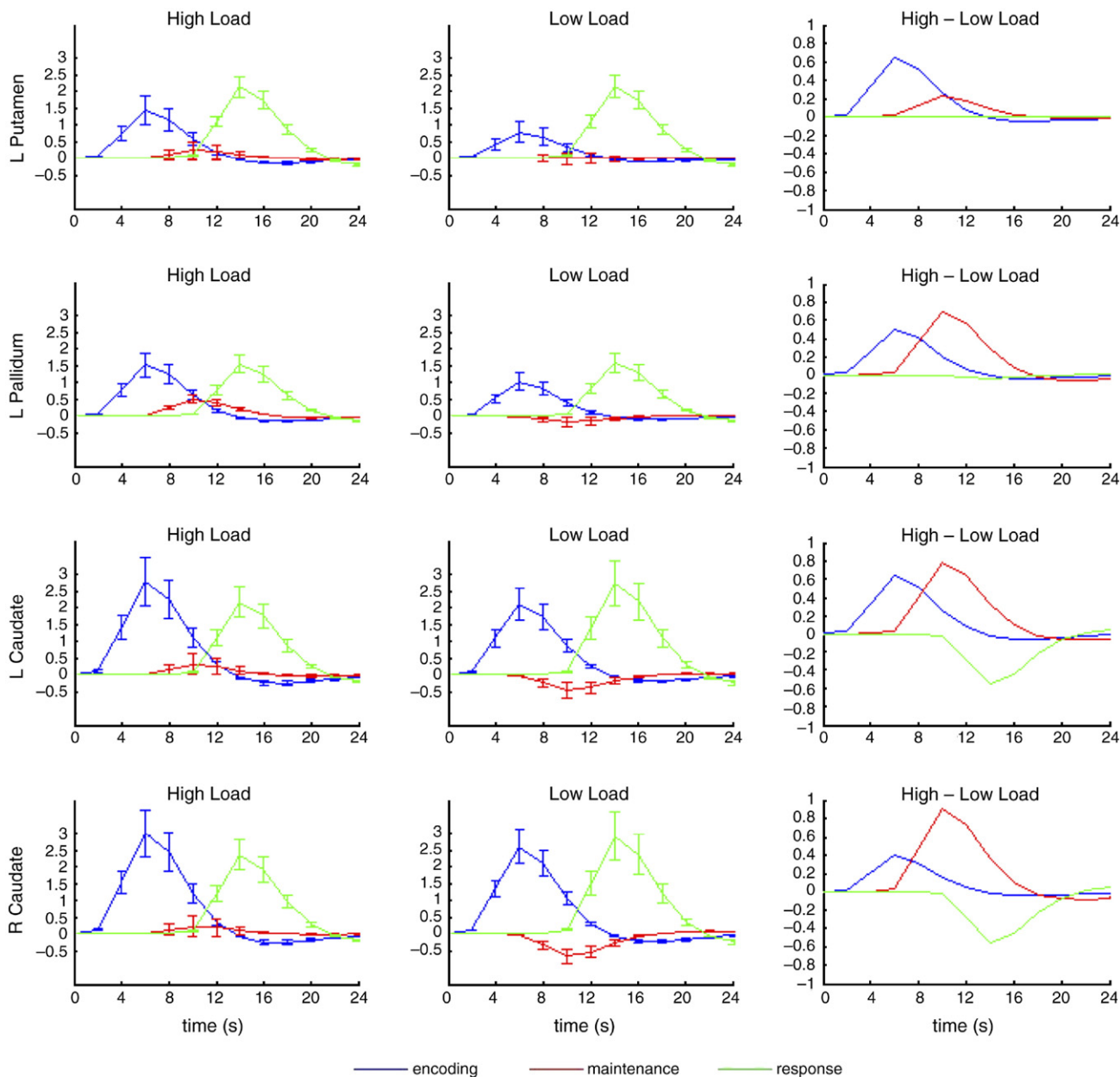


Fig. 5. Time courses of the left putamen, left pallidum, left caudate and right caudate during the encoding (blue), maintenance (red) and response (green) phases for the high-load WM condition (left column), the low-load WM condition (center column) and for the direct comparison high- minus low-load WM conditions (right column). The time courses for the encoding, maintenance and response events were computed separately for each of 14 subjects using the MarsBar toolbox (<http://marsbar.sourceforge.org>); they were then averaged and plotted with error bars at each time point. The time courses of all four ROIs indicate stronger activation during the high-load, compared to low-load, WM condition during the encoding and maintenance phases. During the response phase, basal ganglia responses were strong but not load-dependent.

Table 1A  
Brain regions that showed significant WM-load-dependent activation during the *encoding phase*

Region	Brodmann area	Corrected <i>p</i> value	# of voxels	Peak Z score	Peak MNI coordinates		
					<i>x</i>	<i>y</i>	<i>z</i>
<i>Left hemisphere</i>							
L sup parietal	7	0.001	137	3.69	-28	-60	54
L sup/mid occipital	7/19	<0.001	161	3.87	-30	-74	30
L mid occipital/temporal	19/37	<0.001	418	4.57	-36	-86	-2
L fusiform/inf occipital	19/37			4.06	-42	-60	-14
L insula	47/48	0.003	124	3.22	-34	6	-6
L putamen/L caudate		<0.001	228	3.87	-18	8	-10
L putamen				3.85	-18	8	4
L pallidum				3.17	-24	2	4
<i>Right hemisphere</i>							
R angular/sup occipital	7	0.007	112	3.98	32	-74	44
R mid occipital	19			3.51	30	-82	34
R inf occipital, R fusiform	19	0.007	112	3.84	40	-80	-14

condition during both the encoding and maintenance phases. The left anterior putamen showed the strongest WM load effects during the encoding phase, while those of the left and right caudate and

globus pallidus were strongest during the maintenance phase. No WM-load-dependent activations were observed during the response phase. Analysis of the time courses suggests that these

Table 1B  
Brain regions that showed significant WM-load-dependent activation during the *maintenance phase*

Region	Brodmann area	Corrected <i>p</i> value	# of voxels	Peak Z score	Peak MNI coordinates		
					<i>x</i>	<i>y</i>	<i>z</i>
<i>Left hemisphere</i>							
L/R SMA	6	<0.001	1276	5.47	0	4	62
L mid frontal, L inf frontal operc/tri, L precentral	45/44/48/6	<0.001	3188	4.91	-56	18	12
L inf frontal tri	48				-42	20	18
L insula	48				-32	24	6
L putamen					-20	10	-4
L pallidum					-18	-2	4
L caudate					-18	-14	22
L thalamus					-16	-10	16
L sup parietal	7	<0.001	1327	4.77	-22	-66	44
L inf parietal	40				-50	-42	56
L mid occipital	19				-28	-64	30
L inf occipital	19	<0.001	191	4.77	-52	-70	-12
L sup temporal pole	41	<0.001	202	4.03	-42	-40	22
L cerebellum crus1	18	<0.001	229	4.71	-16	-66	-30
L cerebellum crus1	18				-8	-78	-18
L lingual	17				-4	-74	-6
L cerebellum crus2		0.005	113	4.04	-38	-60	-40
<i>Right hemisphere</i>							
R sup/mid frontal, precentral	6/8	<0.001	218	4.15	30	0	50
R inf frontal tri	45	<0.001	366	3.97	44	38	10
R frontal mid	45				46	42	30
R inf frontal operc, R precentral	44	<0.001	338	4.13	50	14	36
R inf orb frontal, R insula	47	0.001	143	4.14	38	30	-6
R postcentral	3	<0.001	295	4.25	44	-28	50
R supramarginal	2				54	-30	48
R inf parietal	40				52	-38	48
R parietal sup	7	<0.001	393	3.96	34	-72	52
R angular	40				30	-52	34
R occipital sup/mid	7				32	-66	40
R cerebellum 8		<0.001	207	4.08	24	-54	-42
R cerebellum 6	19				28	-68	-26
R thalamus/r caudate		<0.001	288	3.83	10	-32	6

Table 1C

Brain regions that showed significant WM-load-dependent activation during the *response phase*

Region	Brodmann area	Corrected <i>p</i> value	# of voxels	Peak Z score	Peak MNI coordinates		
					<i>x</i>	<i>y</i>	<i>z</i>
<i>Left hemisphere</i>							
L occipital mid	40/7	<0.001	330	3.86	-30	-56	38
L inf parietal	40			3.85	-46	-50	42
L inf parietal	40			3.82	-36	-54	46
<i>Right hemisphere</i>							
L/R frontal sup medial	8	<0.001	231	4.61	0	36	50
R frontal sup medial	8			3.38	4	30	58
L/R ant/mid							
Cingulate	32			3.65	2	32	38
R angular	39	0.008	110	3.5	42	-60	38
R inf parietal	7			3.03	36	-54	44
R angular	7			3.02	40	-72	48

regions were equally activated during the high-load and low-load WM conditions.

Additionally, during the encoding phase, activation was observed bilaterally in the PPC (BA 7) and lateral temporal–occipital cortex (LOC; BA 19/37), as well as in the left FG (BA 37) and left insula (BA 48). During the maintenance phase, activation was observed bilaterally in the VLPFC (BA 44/45/47), PPC (BA 40/7), precentral (BA 6/44) and SMA (BA 6), as well as in the left thalamus, left insula (BA 48), left middle/inferior occipital cortex (BA 19), left cerebellum (crus1 and crus2) and right cerebellum (Lars regions 6/8). During the response phase, activation was

observed bilaterally in the PPC (BA 7/40), pre-SMA (BA 8), ACC (BA 32) and in the left middle occipital cortex (BA 7/40). Table 1A–1C provides the localizations, peak MNI coordinates and corresponding Brodmann areas of all significant ( $p < 0.01$ , corrected for multiple comparisons) activations during each of the three phases.

#### WM-load-dependent effective connectivity of the basal ganglia

Enhanced load-dependent cortical connectivity with the left anterior caudate seed region was apparent in all three phases of the

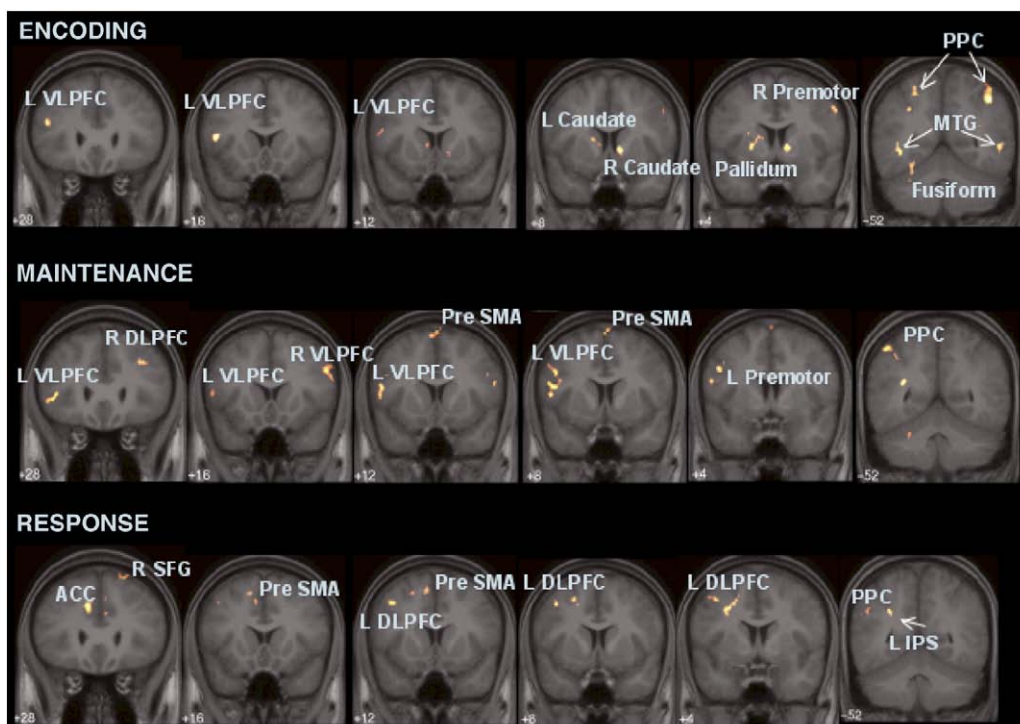


Fig. 6. Brain areas that showed increased WM-load-dependent connectivity with the anterior caudate during the encoding (top), maintenance (middle) and response (bottom) phases. Each cluster is significant at the  $p < 0.05$  uncorrected with a minimum cluster size of 50 voxels. Activations are shown superposed on group-averaged, spatially normalized, T1-weighted structural images. VLPFC: ventral lateral prefrontal cortex; DLPFC: dorsal lateral prefrontal cortex; SMA: supplementary motor area; ACC: anterior cingulate cortex; MTG: medial temporal gyrus; IPS: intraparietal sulcus; SFG: superior frontal gyrus.

task (Fig. 6), with the strongest effects in the left hemisphere. During the encoding phase, left-hemisphere connections were observed with the left VLPFC (BA 47), motor cortex (BA 4), PPC (BA 40/7), FG, MTG/ITG (BA 37), LOC (BA 19) and cerebellum. In the right hemisphere, connections were observed with the motor cortex (BA 4), caudate and thalamus, PPC (BA 40), MTG/ITG (BA 37) and LOC (BA 19). During the maintenance phase, connectivity was observed with the left VLPFC (BA 44/47), pre-SMA (BA 6), SMA (BA 6), PPC (BA 40/7) and cerebellum (6/8). In the right hemisphere, connections were observed with the DLPFC (BA 46), VLPFC (BA 44/45), PPC (BA 7/19), cerebellum (crus1), thalamus and posterior cingulate cortex. During the response phase, connectivity was observed with the left SMA (BA 6), DLPFC (BA 32), ACC (BA 24) and PPC (BA 40). In the right, connectivity was observed with the PPC (BA 40) and superior frontal gyrus (BA 8). Table 2A–2C provides the localizations, peak MNI coordinates and corresponding Brodmann areas for all significant ( $p < 0.05$ , uncorrected due to the limited search volumes) regions demonstrating load-dependent effective connectivity with the seed ROI during each of the three phases. Note that the inclusive masks for each phase encompass, and extend beyond, the regions of significant activation reported at the  $p < 0.01$  level in the section WM-load-related activation in each phase.

Fig. 7 further illustrates the load-dependent increase in connectivity between the caudate and the left DLPFC during the response phase. For each subject, we extracted the mean time series from both the left anterior caudate (seed ROI) and the left DLPFC cluster exhibiting the strongest connectivity with the seed region during the response phase (peak coordinate:  $(-42, 14, 40)$ , cluster size = 88 voxels). The time series were de-meaned, corrected for linear trends and smoothed with the canonical HRF kernel. Samples corresponding to BOLD activity during the response phase of each trial were extracted from both time series and plotted against one another (Fig. 7a). Points corresponding to low-load trials are shown in blue, and those corresponding to high-load trials are shown in red. The linear regression line is superimposed on the scatterplot. Slopes of the regression lines

from the low-load and high-load conditions were computed (Fig. 7b) and entered into a Wilcoxon sign-rank test, yielding a significant difference ( $p < 0.0001$ ).

## Discussion

To our knowledge, this is the first detailed analysis of BG response and connectivity during the encoding, maintenance and retrieval phases of the Sternberg WM task. Our study helps to resolve inconsistencies regarding the role of the BG during WM and, more importantly, provides new insight into the integrative role of the associative regions of the BG.

By directly comparing fMRI responses to a high-load WM task with a low-load WM task, rather than a simple sensorimotor task, we have shown that the BG are specifically involved in verbal, non-spatial, WM. In our modified version of the Sternberg task, the stimuli to be encoded in WM were not presented at multiple spatial locations; therefore, our results cannot be attributed to eye movements or saccades that might have been induced during the encoding phase (Hikosaka et al., 2000). Our control task also allowed us to match for low level sensory and motor processing. Importantly, both tasks required the same set of task rules, so subjects did not have to switch to a non-WM type of control task.

As we discuss below, our analyses suggest load-dependent BG activation and connectivity patterns that are consistent with known human neuroanatomy (Postuma and Dagher, 2006) and animal physiological studies and provide new insights into the dynamic functions of the BG. We emphasize that our study tests for load-dependent responses; that is, regions involved in WM that do not show significant load-dependent activity will be subtracted out and are not considered here. The load-dependent cortical activation averaged across all phases is consistent with previous studies, many of which have compared a WM condition with a non-mnemonic condition (Gruber and von Cramon, 2003); however, as shown in Fig. 3, the use of a tighter control condition in our study ensures more focal responses in the DLPFC, VLPFC, PPC (including the IPS), the fusiform gyrus and the cerebellum (Kirschen et al., 2005).

Table 2A

Brain regions that showed significant WM-load-dependent effective connectivity with the left anterior caudate during the *encoding phase*

Regions	Brodmann areas	Uncorrected $p$ value	# of voxels	Peak Z score	Peak MNI coordinates		
					$x$	$y$	$z$
<i>Left hemisphere</i>							
L inf frontal operc/tri	47/48	0.044	53	3.38	-46	16	12
L postcentral	4	0.003	140	3.43	-46	-8	28
L mid/inf temporal	37	0.01	94	2.83	-44	-52	6
L inf parietal, L angular	40/7	0.025	68	2.98	-40	-58	56
L mid occipital	19	0.006	113	3.34	-38	-88	2
L sup/mid occipital, l cuneus	19	0.007	106	3.16	-14	-70	24
L pallidum/putamen		0.003	135	3.1	-20	2	8
L cerebellum crus1, L fusiform		<0.001	204	3.83	-28	-66	-20
<i>Right hemisphere</i>							
R mid temporal	37	0.014	85	3.26	-56	2	52
R inf parietal, R angular	40	<0.001	244	3.23	-52	48	44
R mid/inf occipital	19	0.01	94	3.31	-80	-2	42
R mid occipital, R cuneus	19	0.003	139	3.42	-70	30	28
R precentral, R postcentral	6/4	0.004	126	3.43	-2	30	52
R caudate/thalamus		0.037	58	1.91	12	-6	14

Table 2B

Brain regions that showed significant WM-load-dependent effective connectivity with the left anterior caudate during the *maintenance phase*

Regions	Brodmann areas	Uncorrected <i>p</i> value	# of voxels	Peak Z score	Peak MNI coordinates		
					<i>x</i>	<i>y</i>	<i>z</i>
<i>Left hemisphere</i>							
L/R SMA	6	0.004	131	3.24	0	-8	58
L precentral, L inf frontal operc	6/44/48	0.001	198	3.34	-50	10	14
L postcentral	48	0.033	63	3.13	-58	-14	26
L inf frontal tri	47	0.024	72	2.82	-46	28	0
L inf parietal, L angular	40/7	0.013	90	3.18	-40	-64	44
L mid temporal	20	0.049	52	2.88	-64	-30	-10
L mid/inf occipital, L inf temp, L fusiform	37	0.039	58	2.76	-46	-64	2
L cerebellum 8		0.047	53	2.93	-10	-66	-38
L cerebellum 6		0.047	53	2.44	-28	-50	-30
L caudate		0.038	59	2.94	-20	-8	24
L putamen		0.047	53	3.38	-28	-20	6
<i>Right hemisphere</i>							
R angular, R sup/mid occipital	7/19	0.003	144	3.31	34	-72	38
R sup frontal	32	0.036	60	3.18	16	38	42
R mid frontal, R inf frontal tri	46/45	0.033	63	2.5	36	28	32
R inf frontal operc	44	0.01	98	2.89	54	18	32
R thalamus/R caudate		0.006	116	3.67	18	-18	18

*WM-load-dependent involvement of the caudate, putamen and globus pallidus*

Significant BG activations specific to WM load were detected in the caudate, putamen and globus pallidus during both the encoding and the maintenance phases, but not during the response phase. Our findings are consistent with previous reports of BG involvement in non-spatial WM tasks (Chein and Fiez, 2001; Manoach et al., 2003; Cairo et al., 2004; Crottaz-Herbette et al., 2004; Lewis et al., 2004) and extend previous findings of BG activation during WM in four important ways.

First, we provide a more detailed quantification of WM-related changes in specific BG nuclei. Converging evidence from voxel-based and time series-based analyses confirmed different patterns of BG responses during the three phases of the WM task. The left and right caudate and globus pallidus exhibited the strongest load-dependent activation during the maintenance phase, while the left anterior putamen exhibited the strongest load-dependent activation during the encoding phase. All four regions were equally active during the high-load and low-load WM conditions during the

response phase, consistent with the role of these regions in motor planning.

Secondly, we have shown that encoding- and maintenance-related activation occurs in the caudate, putamen and globus pallidus. In a prior memory-guided motor task, Menon et al. (2000) reported activation in the putamen and the globus pallidus, but it was unclear how specifically the activations were related to WM maintenance. Cairo et al. (2004) showed increased bilateral activation in the caudate, putamen and globus pallidus with increasing WM load during the encoding phase, and in the putamen during the maintenance phase. Our results extend the findings of Cairo et al. and demonstrate that activation in the anterior caudate and globus pallidus, as well as the putamen, reflects maintenance-related processes, a finding that is consistent with monkey electrophysiological studies (Mushiake and Strick, 1995; Watanabe et al., 2003). Manoach et al. detected activation of the globus pallidus during the response phase and no BG activation during the encoding and maintenance phases. These discrepancies may reflect differences in the HRF model and baseline conditions used in the analysis, as well as differences in the timing parameters

Table 2C

Brain regions that showed significant WM-load-dependent effective connectivity with the left anterior caudate seed ROI during the *response phase*

Regions	Brodmann areas	Uncorrected <i>p</i> value	# of voxels	Peak Z score	Peak MNI coordinates		
					<i>x</i>	<i>y</i>	<i>z</i>
<i>Left hemisphere</i>							
L SMA, L sup frontal	32	<0.001	235	3.45	-16	20	46
L mid frontal, L precentral	44/6	0.016	88	2.83	-42	14	40
L ant cingulate	32	0.007	117	3.32	-12	30	28
L inf parietal, L angular, L supramarg	40	0.004	137	3.35	-48	28	36
L mid occipital	7	0.049	55	3.46	-28	-54	32
<i>Right hemisphere</i>							
R sup frontal	8	0.015	91	3.92	20	32	56
R ant/mid cingulate	32	0.011	100	2.93	6	36	34
R angular, R supramarg, R sup temporal	40/42	0.017	87	2.96	54	-48	26

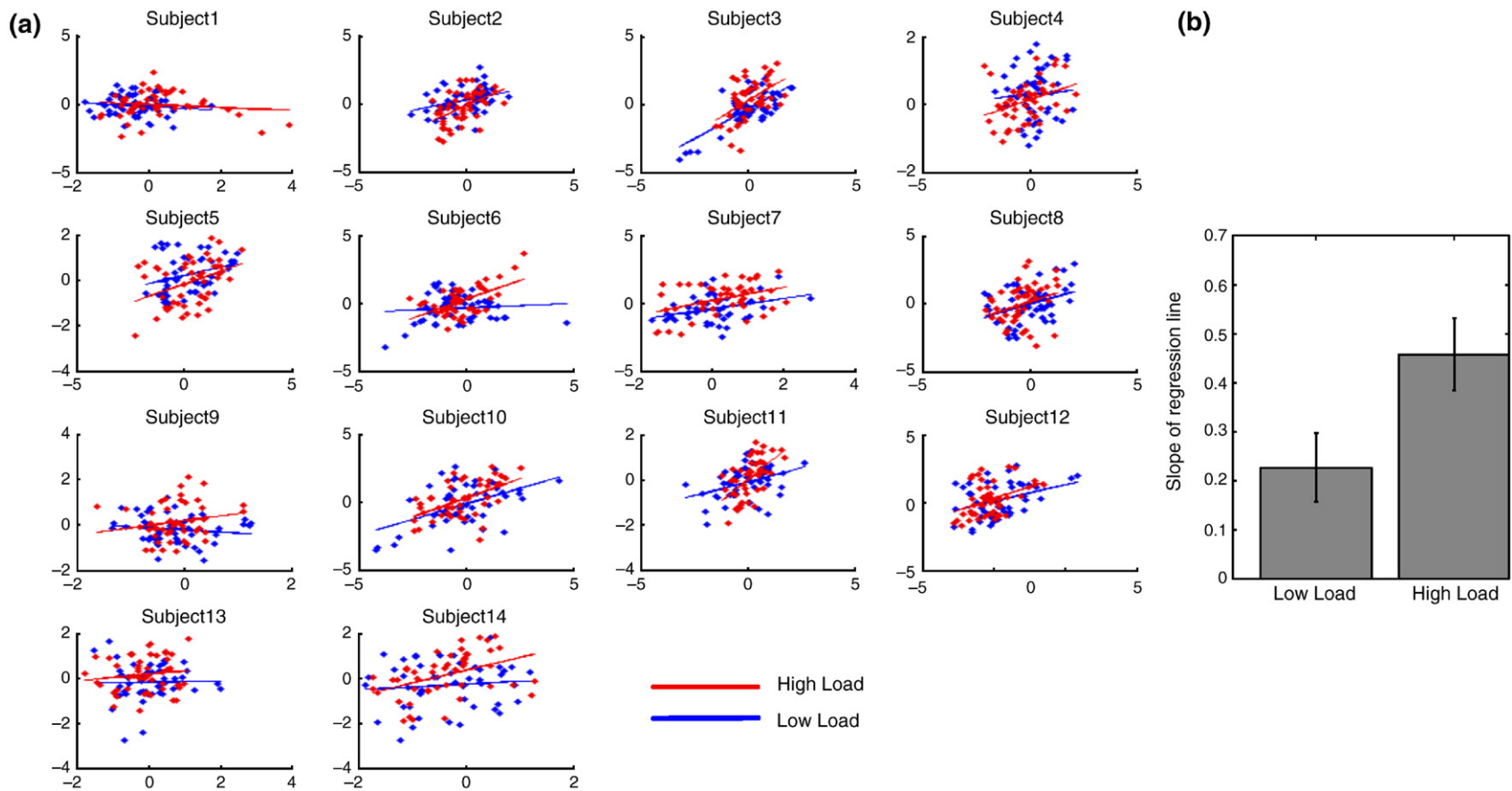


Fig. 7. (a) Illustration of anterior caudate–DLPFC interaction during the response phase as a function of WM load. Scatterplots for each of the 14 subjects, showing the relationship between response phase time points from the anterior caudate seed ROI and response phase time points from a cluster in the left DLPFC (peak coordinate:  $(-42, 14, 40)$ , cluster size=88 voxels). Data points corresponding to BOLD activity during the *response* phase of each trial were extracted from both regions and plotted against one another (*x*-axis: caudate; *y*-axis: DLPFC). Linear regression lines for low-load (blue) and high-load (red) time points are superimposed on the scatterplots. For each subject, the mean time series in both ROIs were de-meaned, corrected for linear trends and filtered (with the canonical HRF kernel) to remove high-frequency noise. (b) Mean and standard error of the linear regression slopes in the low-load and high-load WM conditions during the response phase. The difference in slopes is highly significant ( $p < 0.0001$ ; Wilcoxon sign-rank test) and further demonstrates the strong WM-dependent connectivity between the anterior caudate and DLPFC during the response phase.

of the tasks, such as the length of the maintenance phase. Manoach et al. used an FIR model of the HRF rather than a canonical response shape. In addition, they did not examine load-dependent increases in activation; rather, activation in the encoding phase was compared to a fixation baseline interval, and activation during the response phase was compared to activation during the maintenance phase. Furthermore, Manoach et al. varied the delay phase between 0 and 4 s and did not vary the number of items (load).

Thirdly, in addition to the BG, WM-related responses were detected in the thalamus during the maintenance phase. This may reflect greater outflow from the BG to neocortical regions since the thalamus is the main target site for signals from the globus pallidus (Schell and Strick, 1984; Kayahara and Nakano, 1996).

Finally, putamen activations observed in our study mainly cover the anterior putamen; very little activation was observed in the posterior putamen, which receives projections primarily from the motor cortex. Thus, when the motor and sensory aspects of the task are controlled for, the most significant BG responses are in fact seen in the associative parts of the striatum (Postuma and Dagher, 2006). Taken together, our findings emphasize the critical role of the anterior or associative parts of the BG in WM-load-dependent encoding, maintenance and retrieval.

#### *Anterior caudate interaction with the prefrontal cortex and posterior parietal cortex*

Another novel finding of our study is that the caudate demonstrated strong WM-load-dependent interactions with the neocortex. We used an effective connectivity analysis to examine the interactions of the left anterior caudate in each of the three phases of the WM task. By controlling for sensory and motor control processes, as well as low level encoding and maintenance, we could examine BG connectivity associated with increasing WM load. It is important to reiterate that our connectivity analysis was designed to determine which brain regions have a stronger interaction with the anterior caudate during the high-load, compared to the low-load, WM condition. More widespread connectivity was observed in the ipsilateral (left) hemisphere, consistent with known anatomical projections (Strafella et al., 2001, 2003). Hence, we choose here to focus our discussion on key regions in the left hemisphere with which the caudate demonstrated strong WM-load-dependent interactions. We found that the left anterior caudate showed strong WM-related interactions with the left VLPFC, FG, ITG and the PPC during the encoding phase; with the left VLPFC, pre-SMA, pre-motor cortex and PPC during the maintenance phase; and with the left DLPFC, ACC, pre-SMA and left PPC during the response phase. The key findings here are summarized in Table 3.

Table 3  
Effective connectivity of the left anterior caudate with key cortical regions in the left hemisphere

	Encoding	Maintenance	Response
VLPFC	Yes	Yes	No
PPC	Yes	Yes	Yes
FG/ITG	Yes	No	No
Pre-SMA	No	Yes	Yes
DLPFC	No	No	Yes
ACC	No	No	Yes

It is well known that there are at least five different BG–thalamo–cortical loops which play important roles in sensorimotor, associative, oculo-motor and limbic information processing (Alexander et al., 1986, 1990). Of these loops, the sensorimotor and associative circuits are relevant to our study. In particular, electrophysiological and anatomic studies on non-human primates have shown that the VLPFC and DLPFC project to the caudate and to the anterior regions of the putamen and that the premotor and motor cortices are the targets of BG output projections through the globus pallidus and the thalamus (Selemon and Goldman-Rakic, 1985; Alexander et al., 1990; Parent and Hazrati, 1995; Middleton and Strick, 2000). These cortico-subcortical loops involving BG appear to be organized in a similar way in humans; indeed, recent diffusion tensor imaging-based fiber tracking showed that the anterior (associative), posterior (sensorimotor) and ventral (limbic) compartments of the human striatum have specific connections with the cortex, particularly the frontal lobes (Lehericy et al., 2004).

Our results correspond well with the associative part of the BG circuit described above (Postuma and Dagher, 2006) and are also consistent with recent evidence regarding the dissociable roles of the VLPFC and DLPFC in WM. The left caudate showed increased WM-load-dependent connectivity with the left VLPFC during the encoding and maintenance phases, but not during the response phase of the task. On the other hand, strong connectivity with the left DLPFC was present only during the response phase. The VLPFC and DLPFC are thought to play an important role in WM, although their precise role in the organization of information, interference resolution and selective retrieval versus maintenance and manipulation of information in WM is not entirely clear (Duncan and Owen, 2000; Fletcher and Henson, 2001). One emerging view is that the VLPFC is important for maintaining information in WM, whereas the DLPFC is more critically involved in manipulation of items that are active in WM (Petrides, 2000; Ranganath, 2006). Our data extend these results in new ways by suggesting that caudate–DLPFC interactions are strongest when the current stimulus set has to be matched with an incoming stimulus and when the current stimulus set is more complex. Ipsilateral caudate–DLPFC connectivity during the response phase is consistent with a repetitive transcranial magnetic stimulation study (Strafella et al., 2001) and may be related to decision-making processes initiated by the probe, such as mentally scanning the items maintained in WM, comparing them to the probe and selecting the appropriate motor response (Manoach et al., 2003). Furthermore, the ACC, which is another key region involved in response selection and attentional control (Milham et al., 2003; Crottaz-Herbette and Menon, 2006), also showed stronger connectivity with anterior caudate only during the probe/response phase. On the other hand, connectivity between the caudate and the VLPFC appears to be primarily driven by the requirements of encoding and maintenance in WM.

The anterior caudate also showed WM-load-dependent interaction with the PPC during all three phases of the task. The inferior PPC is known to serve as a short-term visual buffer (Todd and Marois, 2004), both as a graphemic buffer (presumably mediated by the right PPC) and a phonological buffer (mediated by the left PPC). It is notable that, during the maintenance phase, the WM-load-related interaction effects were primarily localized to the left PPC, a region that is involved in maintenance of WM information in a phonological buffer (Shallice, 1988; Cohen, 1992; Paulesu et al., 1993; Awh et al., 1996; Fiez et al., 1996; Jonides et al., 1998;

Henson et al., 2000; Crottaz-Herbette et al., 2004). This suggests a mechanism by which the caudate may help to encode information into phonological representations.

During the maintenance and response phases, the anterior caudate also showed increased connectivity with the left pre-SMA. This finding is consistent with diffusion tensor imaging studies in humans showing connectivity of the pre-SMA with rostral or associative parts of the striatum, including the caudate head (Lehericy et al., 2004); it is also consistent with fMRI studies implicating the pre-SMA in visuo-motor associations, preparation and motor sequencing (Hikosaka et al., 1996; Humberstone et al., 1997; Sakai et al., 1999). The pre-SMA in turn is known to be tightly coupled to the DLPFC (Picard and Strick, 2001; Hoshi and Tanji, 2004), and their mutual interaction may facilitate cognitive control over response selection.

Physiological and computational models suggest that one mode of BG function is to serve as a “brake” on the thalamus, such that neocortical excitation of the caudate nucleus (via either the PPC or the PFC) may lead to disinhibition of the thalamus (Parent and Hazrati, 1995; Middleton and Strick, 2000). This could facilitate reverberant activation in fronto-parietal loops (Ashby et al., 2005) thereby contributing to the maintenance of information in WM. In this manner, the caudate may provide a dynamic gating mechanism for controlling and updating WM (O’Reilly and Frank, 2006). Consistent with this view, our findings suggest that the caudate may gate different functional circuits during the three phases of the Sternberg WM task. Taken together, our findings provide new evidence for a dynamic sequence of context-dependent and regionally specific responses and interactions involving the BG. More generally, our study further underscores the important role played by the BG in adaptive processing of distributed information in a manner that facilitates the transformation of sensory input and cognitive operations into behavior (Graybiel, 2004).

## Acknowledgments

The authors thank Valorie Salimpoor for assistance with the figures, Drs. Jonathan Taylor and John Desmond for helpful discussions concerning statistical analysis of the event-related fMRI data, Robert Anagnoson for assistance with data acquisition, and three anonymous reviewers for helpful comments and suggestions. This research was supported by a Stanford Graduate Fellowship and NSF Graduate Fellowship to CC, a Swiss National Science Foundation fellowship to SCH and by NIH grants HD40761, MH62430 and HD047520 to VM.

## Appendix A. Supplementary data

Supplementary data associated with this article can be found, in the online version, at doi:10.1016/j.neuroimage.2006.08.056.

## References

- Aldridge, J.W., Berridge, K.C., 1998. Coding of serial order by neostriatal neurons: a “natural action” approach to movement sequence. *J. Neurosci.* 18 (7), 2777–2787.
- Alexander, G.E., DeLong, M.R., et al., 1986. Parallel organization of functionally segregated circuits linking basal ganglia and cortex. *Annu. Rev. Neurosci.* 9, 357–381.
- Alexander, G.E., Crutcher, M.D., et al., 1990. Basal ganglia–thalamocortical circuits: parallel substrates for motor, oculomotor, “prefrontal” and “limbic” functions. *Prog. Brain Res.* 85, 119–146.
- Apicella, P., Scarnati, E., et al., 1992. Neuronal activity in monkey striatum related to the expectation of predictable environmental events. *J. Neurophysiol.* 68 (3), 945–960.
- Armstrong, I.T., Chan, F., et al., 2002. Control of saccades in Parkinson’s disease. *Brain Cogn.* 49 (2), 198–201.
- Ashby, F.G., Ell, S.W., et al., 2005. FROST: a distributed neurocomputational model of working memory maintenance. *J. Cogn. Neurosci.* 17 (11), 1728–1743.
- Awh, E., Jonides, J., et al., 1996. Dissociation of storage and rehearsal in verbal working memory. *Psychol. Sci.* 7 (1), 25–31.
- Baddeley, A., 1997. *Human Memory: Theory and Practice*. Oxford Univ. Press, New York.
- Baddeley, A., 2003. Working memory: looking back and looking forward. *Nat. Rev. Neurosci.* 4 (10), 829–839.
- Battig, K., Rosvold, H.E., et al., 1960. Comparison of the effects of frontal and caudate lesions on delayed response and alternation in monkeys. *J. Comp. Physiol. Psychol.* 53, 400–404.
- Bradley, V.A., Welch, J.L., et al., 1989. Visuospatial working memory in Parkinson’s disease. *J. Neurol. Neurosurg. Psychiatry* 52 (11), 1228–1235.
- Braver, T.S., Cohen, J.D., et al., 1997. A parametric study of prefrontal cortex involvement in human working memory. *NeuroImage* 5 (1), 49–62.
- Brett, M., 2000. The MNI Brain and the Talairach Atlas. <http://www.mrc-cbu.cam.ac.uk/Imaging/mnispace.html>.
- Cairo, T., Liddle, P., et al., 2004. The influence of working memory load on phase specific patterns of cortical activity. *Brain Res. Cogn. Brain Res.* 21, 377–387.
- Chein, J.M., Fiez, J.A., 2001. Dissociation of verbal working memory system components using a delayed serial recall task. *Cereb. Cortex* 11 (11), 1003–1014.
- Cohen, S., 1992. *Conduction Aphasia*. Lawrence Erlbaum Associates, Hillsdale, N.J.
- Cohen, J.D., MacWhinney, B., et al., 1993. PsyScope: a new graphic interactive environment for designing psychology experiments. *Behav. Res. Methods Instrum. Comput.* 25, 257–271.
- Cooper, J.A., Sagar, H.J., et al., 1991. Cognitive impairment in early, untreated Parkinson’s disease and its relationship to motor disability. *Brain* 114 (Pt 5), 2095–2122.
- Crottaz-Herbette, S., Menon, V., 2006. “Where and when the anterior cingulate cortex modulates attentional response”. *J. Cogn. Neurosci.* 18 (5), 766–780.
- Crottaz-Herbette, S., Anagnoson, R.T., et al., 2004. Modality effects in verbal working memory: differential prefrontal and parietal responses to auditory and visual stimuli. *NeuroImage* 21 (1), 340–351.
- Dagher, A., Owen, A.M., et al., 2001. The role of the striatum and hippocampus in planning: a PET activation study in Parkinson’s disease. *Brain* 124 (Pt 5), 1020–1032.
- Dean, W.H., Davis, G.D., 1959. Behavior changes following caudate lesions in rhesus monkey. *J. Neurophysiol.* 22, 525–537.
- D’Esposito, M., Aguirre, G.K., et al., 1998. Functional MRI studies of spatial and nonspatial working memory. *Brain Res. Cogn. Brain Res.* 7 (1), 1–13.
- Divac, I., Rosvold, H.E., et al., 1967. Behavioral effects of selective ablation of the caudate nucleus. *J. Comp. Physiol.* 63, 184–190.
- Duncan, J., Owen, A.M., 2000. Common regions of the human frontal lobe recruited by diverse cognitive demands. *Trends Neurosci.* 23 (10), 475–483.
- Duvernoy, H.M., Bourgouin, P., et al., 1999. *The Human Brain: Functional Anatomy, Vascularization and Serial Sections with MRI*. Springer, NY.
- Elliott, R., Dolan, R.J., 1999. Differential neural responses during performance of matching and nonmatching to sample tasks at two delay intervals. *J. Neurosci.* 19 (12), 5066–5073.
- Fiez, J.A., Raife, E.A., et al., 1996. A positron emission tomography study of the short-term maintenance of verbal information. *J. Neurosci.* 16 (2), 808–822.

- Fletcher, P.C., Henson, R.N., 2001. Frontal lobes and human memory: insights from functional neuroimaging. *Brain* 124 (Pt 5), 849–881.
- Friston, K.J., Holmes, A.P., et al., 1995. Statistical parametric maps in functional imaging: a general linear approach. *Hum. Brain Mapp.* 2, 189–210.
- Friston, K.J., Buechel, C., et al., 1997. Psychophysiological and modulatory interactions in neuroimaging. *NeuroImage* 6 (3), 218–229.
- Funahashi, S., Bruce, C.J., et al., 1989. Mnemonic coding of visual space in the monkey's dorsolateral prefrontal cortex. *J. Neurophysiol.* 61 (2), 331–349.
- Gazzaley, A., Rissman, J., et al., 2004. Functional connectivity during working memory maintenance. *Cogn. Affect. Behav. Neurosci.* 4 (4), 580–599.
- Glover, G.H., Lai, S., 1998. Self-navigated spiral fMRI: interleaved versus single-shot. *Magn. Reson. Med.* 39 (3), 361–368.
- Goldman, P.S., Rosvold, H.E., 1972. The effects of selective caudate lesions in infants and juvenile rhesus monkeys. *Brain Res.* 43, 53.
- Goldman-Rakic, P.S., 1999. The physiological approach: functional architecture of working memory and disordered cognition in schizophrenia (In Process Citation) *Biol. Psychiatry* 46 (5), 650–661.
- Graybiel, A.M., 1997. The basal ganglia and cognitive pattern generators. *Schizophr. Bull.* 23 (3), 459–469.
- Graybiel, A.M., 2004. Network-level neuroplasticity in cortico-basal ganglia pathways. *Parkinsonism Relat. Disord.* 10 (5), 293–296.
- Gruber, O., von Cramon, D.Y., 2003. The functional neuroanatomy of human working memory revisited. Evidence from 3-T fMRI studies using classical domain-specific interference tasks. *NeuroImage* 19 (3), 797–809.
- Handwerker, D.A., Ollinger, J.M., et al., 2004. Variation of BOLD hemodynamic responses across subjects and brain regions and their effects on statistical analyses. *NeuroImage* 21 (4), 1639–1651.
- Henson, R.N., Burgess, N., et al., 2000. Recoding, storage, rehearsal and grouping in verbal short-term memory: an fMRI study. *Neuropsychologia* 38 (4), 426–440.
- Hikosaka, O., Sakamoto, M., et al., 1989. Functional properties of monkey caudate neurons III. Activities related to expectation of target and reward. *J. Neurophysiol.* 61 (4), 814–832.
- Hikosaka, O., Sakai, K., et al., 1996. Activation of human presupplementary motor area in learning of sequential procedures: a functional MRI study. *J. Neurophysiol.* 76 (1), 617–621.
- Hikosaka, O., Takikawa, Y., et al., 2000. Role of the basal ganglia in the control of purposive saccadic eye movements. *Physiol. Rev.* 80 (3), 953–978.
- Hoshi, E., Tanji, J., 2004. Differential roles of neuronal activity in the supplementary and presupplementary motor areas: from information retrieval to motor planning and execution. *J. Neurophysiol.* 92 (6), 3482–3499.
- Humberstone, M., Sawle, G.V., et al., 1997. Functional magnetic resonance imaging of single motor events reveals human presupplementary motor area. *Ann. Neurol.* 42 (4), 632–637.
- Jonides, J., Schumacher, E.H., et al., 1998. The role of parietal cortex in verbal working memory. *J. Neurosci.* 18 (13), 5026–5034.
- Kayahara, T., Nakano, K., 1996. Pallido–thalamo–motor cortical connections: an electron microscopic study in the macaque monkey. *Brain Res.* 706 (2), 337–342.
- Kirschen, M.P., Chen, S.H., et al., 2005. Load- and practice-dependent increases in cerebro-cerebellar activation in verbal working memory: an fMRI study. *NeuroImage* 24 (2), 462–472.
- Lehericy, S., Ducros, M., et al., 2004. 3-D diffusion tensor axonal tracking shows distinct SMA and Pre-SMA projections to the human striatum. *Cereb. Cortex* 14 (12), 1302–1309.
- Lewis, S.J., Dove, A., et al., 2003. Cognitive impairments in early Parkinson's disease are accompanied by reductions in activity in frontostriatal neural circuitry. *J. Neurosci.* 23 (15), 6351–6356.
- Lewis, S.J., Dove, A., et al., 2004. Striatal contributions to working memory: a functional magnetic resonance imaging study in humans. *Eur. J. Neurosci.* 19 (3), 755–760.
- Magnotta, V.A., Heckel, D., et al., 1999. Measurement of brain structures with artificial neural networks: two- and three-dimensional applications. *Radiology* 211 (3), 781–790.
- Mai, J.K., Assheuer, J., et al., 1997. *Atlas of the Human Brain*. Academic Press, London.
- Manoach, D.S., Greve, D.N., et al., 2003. Identifying regional activity associated with temporally separated components of working memory using event-related functional MRI. *NeuroImage* 20 (3), 1670–1684.
- Menon, V., Anagnoson, R.T., et al., 2000. Basal ganglia involvement in memory-guided movement sequencing. *NeuroReport* 11 (16), 3641–3645.
- Middleton, F.A., Strick, P.L., 2000. Basal ganglia and cerebellar loops: motor and cognitive circuits. *Brain Res. Brain Res. Rev.* 31 (2–3), 236–250.
- Middleton, F.A., Strick, P.L., 2002. Basal-ganglia 'projections' to the prefrontal cortex of the primate. *Cereb. Cortex* 12 (9), 926–935.
- Milham, M.P., Banich, M.T., et al., 2003. Practice-related effects demonstrate complementary roles of anterior cingulate and prefrontal cortices in attentional control. *NeuroImage* 18 (2), 483–493.
- Mordinov, E.F., 1981. Effect of successive electrical stimulation of different parts of the brain on delayed spatial choice in monkeys. *Neurosci. Behav. Physiol.* 11, 164–169.
- Morris, R.G., Downes, J.J., et al., 1988. Planning and spatial working memory in Parkinson's disease. *J. Neurol. Neurosurg. Psychiatry* 51 (6), 757–766.
- Mushiakhe, H., Strick, P.L., 1995. Pallidal neuron activity during sequential arm movements. *J. Neurophysiol.* 74 (6), 2754–2758.
- Oldfield, R.C., 1971. The assessment and analysis of handedness: the Edinburgh inventory. *Neuropsychologia* 9 (1), 97–113.
- O'Reilly, R.C., Frank, M.J., 2006. Making working memory work: a computational model of learning in the prefrontal cortex and basal ganglia. *Neural Comput.* 18 (2), 283–328.
- Owen, A.M., Evans, A.C., et al., 1996. Evidence for a two-stage model of spatial working memory processing within the lateral frontal cortex: a positron emission tomography study. *Cereb. Cortex* 6 (1), 31–38.
- Owen, A.M., Iddon, J.L., et al., 1997. Spatial and non-spatial working memory at different stages of Parkinson's disease. *Neuropsychologia* 35 (4), 519–532.
- Owen, A.M., Doyon, J., et al., 1998. Abnormal basal ganglia outflow in Parkinson's disease identified with PET. Implications for higher cortical functions. *Brain* 121 (Pt 5), 949–965.
- Parent, A., Hazrati, L.N., 1995. Functional anatomy of the basal ganglia I. The cortico–basal ganglia–thalamo–cortical loop. *Brain Res. Brain Res. Rev.* 20 (1), 91–127.
- Paulesu, E., Frith, C.D., et al., 1993. The neural correlates of the verbal component of working memory. *Nature* 362 (6418), 342–345.
- Petrides, M., 2000. Dissociable roles of mid-dorsolateral prefrontal and anterior inferotemporal cortex in visual working memory. *J. Neurosci.* 20 (19), 7496–7503.
- Petrides, M., Alivisatos, B., et al., 1993. Functional activation of the human frontal cortex during the performance of verbal working memory tasks. *Proc. Natl. Acad. Sci. U. S. A.* 90 (3), 878–882.
- Picard, N., Strick, P.L., 2001. Imaging the premotor areas. *Curr. Opin. Neurobiol.* 11 (6), 663–672.
- Poline, J.B., Worsley, K.J., et al., 1997. Combining spatial extent and peak intensity to test for activations in functional imaging. *NeuroImage* 5 (2), 83–96.
- Postle, B.R., D'Esposito, M., 1999a. Dissociation of human caudate nucleus activity in spatial and nonspatial working memory: an event-related fMRI study. *Brain Res. Cogn. Brain Res.* 8 (2), 107–115.
- Postle, B.R., D'Esposito, M., 1999b. "What"–Then–Where" in visual working memory: an event-related fMRI study. *J. Cogn. Neurosci.* 11 (6), 585–597.
- Postuma, R.B., Dagher, A., 2006. Basal ganglia functional connectivity based on a meta-analysis of 126 positron emission tomography and functional magnetic resonance imaging publications. *Cereb. Cortex* 16 (10), 1508–1521.
- Ranganath, C., 2006. Working memory for visual objects: complementary

- roles of inferior temporal, medial temporal, and prefrontal cortex. *Neuroscience* 139 (1), 277–289.
- Ravizza, S.M., Ivry, R.B., 2001. Comparison of the basal ganglia and cerebellum in shifting attention. *J. Cogn. Neurosci.* 13 (3), 285–297.
- Rosvold, H.E., Delgado, J.M.R., et al., 1956. The effect on delayed-attention test performance of stimulating or destroying electrically structures within the frontal lobes of the monkey's brain. *J. Comp. Physiol. Psychol.* 49, 365–372.
- Rowe, J.B., Toni, I., et al., 2000. The prefrontal cortex: response selection or maintenance within working memory? *Science* 288 (5471), 1656–1660.
- Rypma, B., Prabhakaran, V., et al., 1999. Load-dependent roles of frontal brain regions in the maintenance of working memory. *NeuroImage* 9 (2), 216–226.
- Sakai, K., Hikosaka, O., et al., 1999. Presupplementary motor area activation during sequence learning reflects visuo-motor association. *J. Neurosci.* 19 (10), RC1.
- Schell, G.R., Strick, P.L., 1984. The origin of thalamic inputs to the arcuate premotor and supplementary motor areas. *J. Neurosci.* 4 (2), 539–560.
- Selemon, L.D., Goldman-Rakic, P.S., 1985. Longitudinal topography and interdigitation of corticostriatal projections in the rhesus monkey. *J. Neurosci.* 5 (3), 776–794.
- Shallice, T., 1988. *From Neuropsychology to Mental Structure*. Cambridge Univ. Press, Cambridge U.K.
- Skeel, R.L., Crosson, B., et al., 2001. Basal ganglia dysfunction, working memory, and sentence comprehension in patients with Parkinson's disease. *Neuropsychologia* 39 (9), 962–971.
- Stamm, J.S., 1969. Electrical stimulation of monkeys' prefrontal cortex during delayed-response performance. *J. Comp. Physiol. Psychol.* 67, 535–546.
- Sternberg, S., 1966. High-speed scanning in human memory. *Science* 153 (736), 652–654.
- Strafella, A.P., Paus, T., et al., 2001. Repetitive transcranial magnetic stimulation of the human prefrontal cortex induces dopamine release in the caudate nucleus. *J. Neurosci.* 21 (15), RC157.
- Strafella, A.P., Paus, T., et al., 2003. Striatal dopamine release induced by repetitive transcranial magnetic stimulation of the human motor cortex. *Brain* 126 (Pt 12), 2609–2615.
- Talairach, J., Tournoux, P., 1988. *Co-Planar Stereotaxic Atlas of the Human Brain*. Thieme, Stuttgart, N.Y.
- Todd, J.J., Marois, R., 2004. Capacity limit of visual short-term memory in human posterior parietal cortex. *Nature* 428 (6984), 751–754.
- Watanabe, K., Lauwereyns, J., et al., 2003. Neural correlates of rewarded and unrewarded eye movements in the primate caudate nucleus. *J. Neurosci.* 23 (31), 10052–10057.
- Zarahn, E., Aguirre, G., et al., 1997. A trial-based experimental design for MRI. *NeuroImage* 6 (2), 122–138.